

Large scale structure constraints and matter power spectrum in $f(Q, \mathcal{L}_m)$ gravity

Praveen Kumar Dhankar

*Symbiosis Institute of Technology, Nagpur Campus,
Symbiosis International (Deemed University), Pune-440008, Maharashtra, India*

Albert Munyeshyaka*

*Rwanda Astrophysics Space and Climate Science Research Group,
University of Rwanda, College of Science and Technology, Kigali, Rwanda*

Saddam Hussain

Institute of Theoretical Physics and Cosmology, Zhejiang University of Technology, Hangzhou 310023, China

Tom Mutabazi

Mbarara University of Science and Technology, Mbarara, Uganda.

(Dated: July 16, 2025)

In the present work, we take into account the dynamical system analysis to investigate the matter power spectrum within the framework of the $f(Q, \mathcal{L}_m)$ gravitational theory. After obtaining autonomous dynamical system variables for two different particular pedagogical choices of $f(Q, \mathcal{L}_m)$ models (A and B), we derive the full system of perturbation equations using the $1+3$ covariant formalism to study the matter fluctuations. We present and solve the energy density perturbation equations to obtain the energy density contrast, which decays with redshift for both models for a particular choice of model parameters. After obtaining the numerical results of the density contrast, we computed the matter spectra for each model and conducted a comparative analysis with the Λ CDM. Furthermore, by employing the Markov Chain Monte Carlo (MCMC) analysis, the model parameters were constrained using a combination of different observational data sets to improve the robustness and accuracy of the parameter estimation. Our results indicate that only model A can be compatible with the considered observational data sets.

I. INTRODUCTION

The recent observations present the convincing evidence that the current universe is experiencing an accelerated phase of expansion. Different studies have been trying to explain possible causes of this puzzle, though most of them face many challenges [1].

The most acceptable model in trying to explain the cause of this acceleration is the concordance model dubbed the Λ CDM model, which utilizes the Λ as a source of dark energy. This model agrees with a number of observations such as Type I_a supernovae [1], cosmic microwave background (CMB) [2–4], Baryon acoustic oscillations (BAO) [5, 6] and large scale structure [7]. Despite the remarkable successes, this model faces different challenges in the early and late time universe such as the fine tuning problems, the problems of Hubble and σ_8 tensions. This has led to a search for alternative theory to explain the possible source of dark energy and in line with observational predictions. Among the leading theory includes the consideration of the geometrical source of dark energy which leads to the consideration of modified theories of gravity such as $f(R)$ [8, 9], $f(G)$ [10, 11], $f(T)$ [12] and $f(Q)$ [13, 14] to name but a few, where R is the Ricci scalar, G is the Gauss-Bonnet invariant, T is the torsion scalar and Q is

the nonmetricity scalar, respectively.

The simplest theory $f(R)$ arises through an extension of the Einstein-Hilbert action by replacing Ricci scalar by an arbitrary function for the Ricci scalar to form the $f(R)$ theory. This theory is able to explain the cosmic accelerated expansion in geometrical way without the need of dark energy and it can explain the flat rotational curves of galaxies [15–19]. However the $f(R)$ theory of gravity faces some challenges for example when subjected to solar system test, and matter instability issues [34, 40].

An alternative method to extending the Einstein-Hilbert action involves postulating the presence of a non-minimal coupling, for example between geometry and matter leading to $f(R, \mathcal{L}_m)$ gravity, geometry and the trace of energy-momentum tensor giving rise to $f(R, T)$ gravity [22–29]. In this case gravitational dynamics is described by more general functions of the curvature scalar, matter Lagrangian and the trace of energy momentum tensor, respectively allowing to investigate gravitational behaviors beyond GR and Λ CDM predictions.

The $f(T)$ gravity theories have been extensively explored in different contexts and distinguished among theories which can explain the cosmic acceleration without the need for dark energy [30–33]. Another alternative theory in a geometrical formulation of gravitation includes the use of nonmetricity Q of the metric explored in different contexts, for examples the work conducted in [34] explored the impact of $f(Q)$ gravity on the large scale

* munalph@gmail.com

structure and the authors investigated the logarithmic $f(Q)$ gravity in terms of observational constraints using Monte-Carlo-Markov-Chain (MCMC) method and high body simulations, whereas in [35], the authors discussed the Solar system tests in covariant $f(Q)$ gravity. This theory offers an advantage of coordinate calculations in GR in a covariant way. Cosmology of $f(Q)$ gravity theory and its observational constraints were analysed in [36–39]. A key aspect of $f(Q)$ gravity theory is that it is possible to distinguish gravity from inertial effects. This theory offers a straightforward formulation in which self-accelerating solutions spontaneously appear in both early and late time universes and has a substantial benefit that the background field equations are always second order and the matter instabilities can be avoided in the $f(Q)$ theory [34, 40].

The $f(Q)$ gravity theory has been explored in a number of studies which confirmed its authenticity in reproducing both the early and the late time dynamics of the universe in a way similar to the Λ CDM model. It can satisfy constraints from different observational probes such as CMB, Supernovae type I_a distance modulus, BAO and Observational Hubble Data set (OHD). Nevertheless, there exists different types of observations that are sensitive not only to the expansion history of the universe but also to the evolution of matter perturbations. The fact that the evolution of perturbations depends on the specific gravity theory has made these observations a key actor in distinguishing between different cosmological models and the mechanism driving cosmic acceleration [62]. In this regard, as far as cosmological perturbation is concerned, the $1+3$ covariant perturbations explored extensively in previous works [42, 62] can be used to obtain energy density perturbation equations. Different works have been considering this formalism in the context of $f(Q)$ gravity to investigate the evolution of large-scale structure. For example, the work conducted in [43] investigated cosmological perturbations in $f(Q)$ gravity and discussed the re-scaling of Newton constant in tensor perturbations. The scalar parts of the perturbations introduced two additional propagating modes, suggesting that $f(Q)$ gravity presents at least two extra degrees of freedom. Moreover, extending non-metric gravity by incorporating the trace of energy-momentum tensor T of matter to formulate $f(Q, T)$ has been investigated in different works. The $f(Q, T)$ theory was observationally constrained and some of the models of the $f(Q, T)$ gravity have successfully described accelerated expansion of the universe [44–47], offering viable alternatives to the standard Λ CDM paradigm.

The work conducted by [48] extended the non-metric gravity by incorporating the matter Lagrangian in the Lagrangian density of the $f(Q)$ gravity to obtain $f(Q, \mathcal{L}_m)$ gravity theory. The authors among other things investigated the conservation problem of the mat-

ter energy momentum tensor, investigated the cosmic evolution for the case of a flat Friedmann-Lemaître-Robertson-Walker metric and further consider two particular gravitational models of in the context of $f(Q, \mathcal{L}_m)$ gravity. The authors compared the evolution of gravitational models with the predictions of two distinct observational data sets.

In the work conducted in [49], the authors investigated late-time cosmology in the context of $f(Q, \mathcal{L}_m)$ gravity and discussed its analytical solutions and observational fits. The authors showed that this theory of gravity contributes to our understanding of the universe’s expansion dynamics.

In [50], $f(Q, \mathcal{L}_m)$ gravity was constrained with bulk viscosity, and the findings underscore the significant role of bulk viscosity in understanding accelerated expansion in the universe within alternative gravity theories.

The work carried out in [51] investigated the observational late-time acceleration in $f(Q, \mathcal{L}_m)$ gravity, and their analysis showed that the $f(Q, \mathcal{L}_m)$ model aligns well with the observational results and exhibits similar behaviours to the Λ CDM model. Motivated by these works, the present work aims to extend the work conducted in [48] to perturbation level to investigate the implications of the considered gravitational models on the evolution of large-scale structure and on the matter power spectrum. In this regards, we use dynamical system approach to obtain autonomous ordinary differential (ODE). We then use the $1+3$ covariant formalism to obtain the energy density perturbation equations. Solving both the autonomous ODEs and the perturbation equations we compute the matter power spectra for each model. The results inform that the effects of the gravitational models considered in this work on the matter power spectra within this $f(Q, \mathcal{L}_m)$ gravity theory provide promising results on the evolution of large scale structure. The next aim is to use MCMC analysis to constrain model parameters resulting from the use of $f(Q, \mathcal{L}_m)$ gravity theory. In so doing, we compute the corner (triangular) plots and present the mean value parameters corresponding to the combinations of data sets namely: (i) CC+PP (ii) CC+DES. For further analysis, we use combinations of redshift space distortion data $f\sigma_8$ data with the latest measurements of the growth rate and amplitude of matter fluctuations σ_8 namely: (iii) CC+BAO+fs8 (iv) CC+BAO+fs8+PP (v) CC+BAO+fs8+DES. Using the MCMC simulations, we are able to constrain the best fit model parameters in the context of $f(Q, \mathcal{L}_m)$ gravity theory.

The rest of this paper is organized as follows: In Section (II), we present the mathematical framework, where cosmological equations are discussed in the context of $f(Q, \mathcal{L}_m)$ gravity and the dynamical system equations for the defined models. In Section (III), we present the covariant density perturbation equations and their corresponding numerical results (energy density contrast). Section (IV) computes and presents the matter power spectra resulting from the energy density perturbation

equations and the dynamical variables of the system for the $f(Q, \mathcal{L}_m)$ gravity models considered, while Section (V) presents the structure growth equation. In Section (VI), we present the data used to constrain model parameters and the results obtained, whereas Section (VII) discusses the results and concludes the work.

II. BACKGROUND AND PERTURBATION EQUATIONS IN $f(Q, \mathcal{L}_m)$ GRAVITY

This section provides an overview of the geometric foundations of the $f(Q, \mathcal{L}_m)$ gravitational theory. We present an action representing this theory, the corresponding gravitational field equations and the conservation equations of the energy momentum tensor. The action principle helps to control the dynamics of a physical system. In the $f(Q, \mathcal{L}_m)$ context, the action is represented as [48–50]

$$S = \int \sqrt{-g} f(Q, \mathcal{L}_m) d^4x, \quad (1)$$

where $\sqrt{-g}$ is the determinant of the metric $g_{\mu\nu}$ and $f(Q, \mathcal{L}_m)$ is an arbitrary function of nonmetricity scalar Q and of matter Lagrangian \mathcal{L}_m . The nonmetricity scalar Q is given by $Q = -Q_{\lambda\mu\nu} P^{\lambda\mu\nu}$ and it describes the deviation of the manifold geometry from isotropy and can be thought of as a measure of how much the volume of a parallelly transported object changes as it moves through space-time, where $P^{\lambda\mu\nu}$ is a super-potential—a nonmetricity conjugate [48, 49]. By varying the action (eq. 1) with respect to the metric tensor and Q and by applying the boundary conditions, integrating and equating the metric variation of the action to zero, one can get the field equations of $f(Q, \mathcal{L}_m)$ gravity as

$$\begin{aligned} \frac{2}{\sqrt{-g}} \nabla_\alpha \left(f_Q \sqrt{-g} P_{\mu\nu}^\alpha \right) + f_Q \left(P_{\mu\alpha\beta} Q_\nu^{\alpha\beta} - 2Q_\mu^{\alpha\beta} P_{\alpha\beta\nu} \right) \\ + \frac{1}{2} f_{\mathcal{L}_m} \left(g_{\mu\nu} \mathcal{L}_m - T_{\mu\nu} \right), \end{aligned} \quad (2)$$

where $T_{\mu\nu} = -\frac{2}{\sqrt{-g}} \frac{\delta(\sqrt{-g} \mathcal{L}_m)}{\delta g^{\mu\nu}}$ is the energy-momentum tensor of the matter, $\delta\sqrt{-g} = -\frac{1}{2} \sqrt{-g} g_{\mu\nu} \delta g^{\mu\nu}$ is the variation of the determinant of the metric and $\delta Q = 2P_{\alpha\nu\rho} \nabla^\alpha \delta g^{\nu\rho} - \left(P_{\mu\alpha\beta} Q_\nu^{\alpha\beta} - 2Q_\mu^{\alpha\beta} P_{\alpha\beta\nu} \right) \delta g^{\mu\nu}$ is the variation of Q . $f_Q = \frac{\partial f(Q, \mathcal{L}_m)}{\partial Q}$ and $f_{\mathcal{L}_m} = \frac{\partial f(Q, \mathcal{L}_m)}{\partial \mathcal{L}_m}$. For the case $f(Q, \mathcal{L}_m) = f(Q) + 2\mathcal{L}_m$, it reduces to the field equations of $f(Q)$ gravity [52]. Consider matter as a perfect fluid, the energy-momentum tensor is presented as

$$T_\nu^\mu = (\rho + p) u_\nu u^\mu + p g_\nu^\mu, \quad (3)$$

where ρ is the energy density and p is the pressure. u^μ denotes the four-velocity of the fluid. In this case, the conservation equation can be written by

$$\dot{\rho} + 3H(\rho + p) = 0. \quad (4)$$

In order to explore the cosmological evolution of the Friedmann-Robert-Walker (FRW) universe in $f(Q, \mathcal{L}_m)$ gravity, let us consider a flat geometry and the space-time metric given by

$$ds^2 = -dt^2 + a(t)^2 (dx^2 + dy^2 + dz^2), \quad (5)$$

where $a(t)$ is the scale factor governing the expansion of the universe, which is related to the Hubble parameter H as $H = \frac{\dot{a}}{a}$. The dot denotes derivative with respect to cosmic time. The nonmetricity is given by $Q = 6H^2$. The non-zero components of the energy-momentum tensor are therefore given by $T_\nu^\mu = (\rho, p, p, p)$. In the following subsection, we present the Friedmann equations in the context of $f(Q, \mathcal{L}_m)$ gravitational theory.

A. Generalised Friedmann equations

Considering the Friedmann-Robert-Walker (FRW) metric in a flat geometry, the Friedmann equations and the continuity equation can be presented, respectively as

$$3H^2 = \rho_{eff}, \quad (6)$$

$$2\dot{H} + 3H^2 = -p_{eff}, \quad (7)$$

$$\dot{\rho}_{eff} + 3H(\rho_{eff} + p_{eff}) = 0, \quad (8)$$

where

$$\rho_{eff} = \frac{1}{4f'} \left[f - f_{lm} (\rho + l_m) \right], \quad (9)$$

$$p_{eff} = 2 \frac{f' H}{f'} - \frac{1}{4f'} \left[f + f_{lm} (\rho + 2p - l_m) \right]. \quad (10)$$

By looking at eq. (6) and eq. (7), the cosmological evolution equations contain extra-terms representing the contributions from non-nonmetricity-matter coupling leading to geometrical dark energy. These terms drive the recent accelerated expansion of the universe.

B. Cosmological models

In this part, we investigate two different cosmological models namely model A and model B given by $f = -\alpha Q + 2l_m + \beta$ and $f = -\alpha Q + (2l_m)^2 + \beta$, respectively explored in [48, 50]. In these works the authors assumed that matter in the universe obeys an equation of state given by $p = (\gamma - 1)\rho$, with $1 \leq \gamma \leq 2$. For $\gamma = \frac{4}{3}$, the equation of state describes the radiation dominated universe, early universe (high density), whereas for $\gamma = 1$, it describes the pressure-less matter (dust).

1. Model A

Consider the model A given by $f = -\alpha Q + 2l_m + \beta$, with $l_m = p$ and $p = (\gamma - 1)\rho$, the Friedmann equations (eq. 6 to eq. 10) reduces to

$$3H^2 = -\frac{\beta}{2\alpha} + \frac{\rho}{\alpha}, \quad (11)$$

$$2\dot{H} + 3H^2 = -3H^2(\gamma - 1) - \frac{\beta\gamma}{2\alpha}, \quad (12)$$

$$\rho_{eff} = \frac{\rho}{2\alpha} - \frac{\beta}{2\alpha}, \quad (13)$$

$$p_{eff} = 3H^2(\gamma - 1) + \frac{\beta\gamma}{2\alpha}, \quad (14)$$

$$H(z) = \left[\frac{(6H_0^2\alpha + \beta)(1+z)^{3\gamma} - \beta}{6\alpha} \right]^{\frac{1}{2}}. \quad (15)$$

In the work conducted by [48], the authors focused mainly on the variables as a function of the redshift of the energy density, deceleration parameter and the effective of equation of state and used MCMC simulations to constrain model parameters. However, in the present we will use the same models to explore the dynamical system and the 1 + 3 covariant perturbations approaches to investigate the effect of each model on large scale structure formation and matter power spectrum. Starting from Eq. (11) and eq. (12), we can find the dynamical system variables.

2. Dynamical system variables for model A

In the present section, we present the dynamical system variables [53–56] in the context of $f(Q, \mathcal{L}_m)$ gravity for model A. From eq. (11) we can rewrite

$$1 = -\frac{\beta}{6\alpha H^2} + \frac{\rho}{3\alpha H^2}, \quad (16)$$

$$1 + x - \Omega_1 - \Omega_2 = 0, \quad (17)$$

$$x = \frac{\beta}{6\alpha H^2}, \quad (18)$$

$$\Omega_1 = \frac{\rho_m}{3\alpha H^2}, \quad (19)$$

$$\Omega_2 = \frac{\rho_r}{3\alpha H^2}. \quad (20)$$

Where $\rho = \rho_m + \rho_r$, $\Omega_1 = \frac{\Omega_m}{\alpha}$ and $\Omega_2 = \frac{\Omega_r}{\alpha}$. From eq. (12), we can get

$$\frac{\dot{H}}{H^2} = -\frac{3}{2}\gamma(x + 1). \quad (21)$$

Using eq. (21) and the fact that $\frac{df}{Hdt} = \frac{df}{dN}$, equations (18), (19) and (20) evolve as

$$\frac{dx}{dN} = -3\gamma x - 3\gamma x^2, \quad (22)$$

$$\frac{d\Omega_1}{dN} = 3\Omega_1(\gamma - 1) + 3\gamma\Omega_1 x, \quad (23)$$

$$\frac{d\Omega_2}{dN} = 3\Omega_2(\gamma - 2) + 3\gamma\Omega_2 x, \quad (24)$$

$$\frac{dh}{dN} = 3h\left(\Omega_2 + \frac{\Omega_1}{2}\right), \quad (25)$$

where $h = \frac{H}{H_0}$, $\dot{\rho}_m = -3H\rho_m$ and $\dot{\rho}_r = -6H\rho_r$. The equations (22), (23), (24) and (25) can be represented in redshift using $\frac{df}{dN} = -(1+z)\frac{df}{dz}$ as

$$-(1+z)\frac{dx}{dz} = -3\gamma x - 3\gamma x^2, \quad (26)$$

$$-(1+z)\frac{d\Omega_1}{dz} = 3\Omega_1(\gamma - 1) + 3\gamma\Omega_1 x, \quad (27)$$

$$-(1+z)\frac{d\Omega_2}{dz} = 3\Omega_2(\gamma - 2) + 3\gamma\Omega_2 x, \quad (28)$$

$$-(1+z)\frac{dh}{dz} = 3h\left(\Omega_2 + \frac{\Omega_1}{2}\right). \quad (29)$$

Eqs. (26)–(29) form an autonomous system of ordinary differential equations of the $f(Q, \mathcal{L}_m)$ gravity in redshift space for the model A. The dimensionality of this system of equations can be reduced using the Friedmann constraint (eq. 17). The evolution of the Hubble parameter (H) was determined using eq. (11) in terms of dynamical system variables. The stability analysis of dynamical variables in the context of $f(Q)$ gravity was conducted in [53]. In this work, the authors showed points corresponding to a deceleration-radiation dominated universe, a deceleration-matter dominated universe and an accelerated dark energy dominated universe. This system of equations (eq. (26)–(29)) together with the energy density perturbation equations (which will be presented in the next sections) will be used to compute the matter power spectrum for model A in $f(Q, \mathcal{L}_m)$ gravity. In the next subsection, let us derive dynamical system equations for the second model dubbed model B

3. Model B

Considering model B defined as $f = -\alpha Q + (2l_m)^2 + \beta$, the Friedmann equations (eq. 6–10) and the Hubble parameter in the $f(Q, \mathcal{L}_m)$ gravity can be modified as

[48]

$$3H^2 = -\frac{2}{\alpha}(1-\gamma^2)\rho^2 - \frac{\beta}{2\alpha}, \quad (30)$$

$$2\dot{H} + 3H^2 = \frac{(\beta + 6\alpha H^2)(\gamma - 1)}{2\alpha(\gamma + 1)} - \frac{\beta}{2\alpha}, \quad (31)$$

$$H(z) = \left[\frac{(6H_0^2\alpha + \beta)(1+z)^{\frac{6\gamma}{1+\gamma}} - \beta}{6\alpha} \right]^{\frac{1}{2}} \quad (32)$$

The dynamical system variables for model B can be obtained by first rewriting the above equation (from eq. 30) as

$$1 = -\frac{\beta}{6\alpha H^2} + \frac{2(\gamma^2 - 1)\rho^2}{3\alpha H^2}, \quad (33)$$

$$1 + y - \Omega_3 - \Omega_4 = 0, \quad (34)$$

$$y = \frac{\beta}{6\alpha H^2}, \quad (35)$$

$$\Omega_3 = \frac{2(\gamma^2 - 1)\rho_m^2}{3\alpha H^2}, \quad (36)$$

$$\Omega_4 = \frac{2(\gamma^2 - 1)\rho_r^2}{3\alpha H^2}. \quad (37)$$

Where $\rho = \rho_m + \rho_r$, $\Omega_3 = 2\frac{(\gamma^2 - 1)}{\alpha}\Omega_m$ and $\Omega_4 = 2\frac{(\gamma^2 - 1)}{\alpha}\Omega_r$.

From eq. (31), the ratio of time derivative of H and the square of H can be calculated as

$$\frac{\dot{H}}{H^2} = -\frac{3}{\gamma + 1} - \frac{3y}{\gamma + 1}. \quad (38)$$

Using eq. (30) and the fact that $\frac{df}{Hdt} = \frac{df}{dN}$, the evolution of the dynamical system variables (eq. (35), eq. (36) and Eq. (37)) can be presented as

$$\frac{dy}{dN} = \frac{6y}{\gamma + 1} + \frac{6y^2}{\gamma + 1}, \quad (39)$$

$$\frac{d\Omega_3}{dN} = -3\Omega_3\left(\frac{1+2\gamma}{\gamma+1}\right) + \frac{3\Omega_3 y}{\gamma+1}, \quad (40)$$

$$\frac{d\Omega_4}{dN} = -\frac{3(3+4\gamma)}{\gamma+1} + \frac{3\Omega_4 y}{\gamma+1}, \quad (41)$$

$$\frac{dh}{dN} = 3h(2\Omega_4 + \Omega_3), \quad (42)$$

which can be rewritten in redshift space as

$$-(1+z)\frac{dy}{dz} = \frac{6y}{\gamma+1} + \frac{y^2}{\gamma+1}, \quad (43)$$

$$-(1+z)\frac{d\Omega_3}{dz} = -3\Omega_3\left(\frac{1+2\gamma}{\gamma+1}\right) + \frac{3\Omega_3 y}{\gamma+1}, \quad (44)$$

$$-(1+z)\frac{d\Omega_4}{dz} = -\frac{3(3+4\gamma)}{\gamma+1} + \frac{3\Omega_4 y}{\gamma+1}, \quad (45)$$

$$-(1+z)\frac{dh}{dz} = 3h(2\Omega_4 + \Omega_3). \quad (46)$$

Eqs. (43)–(46) form an autonomous system of ordinary differential equations in the redshift space for model B in $f(Q, \mathcal{L}_m)$ gravity. These equations together with the energy density perturbations will be used to analyse the effect of this model on structure formation and on the matter power spectrum. In the next section, we derive the energy density perturbation equations in the context of $f(Q, \mathcal{L}_m)$ gravity.

III. ENERGY DENSITY PERTURBATION IN $f(Q, \mathcal{L}_m)$ GRAVITY

It is currently a well known fact that the universe is not perfectly smooth, but full of large scale structure such as galaxies, clusters of galaxies and voids, to name but a few. These structures are believed to be the result of primordial fluctuations. Cosmological perturbations provide a room for explaining how structures grow from small fluctuations to large structures we see today in the universe. There are currently two approaches of perturbing—namely, the metric-based approach, developed by Lifshitz [63], Badeen [64]. and the covariant approach developed by Hawking [65] and Ellis and Bruni [66]. These approaches differ in the fact that it is difficult in dealing with non-linear theory and requires that the metric be specified from the start for the metric approach, whereas the covariant formalism helps in describing space-time via covariantly defined variables with respect to a partial frame, such as the 1 + 3 covariant space-time decomposition techniques. It is a suitable method to describe physics and geometry using tensor quantities and relations valid in all coordinate systems. Non-linearities can be accommodated, but the main advantage of the 1+3 covariant approach is that no unphysical gauge modes exist [67–73]. Previous work in the context of $f(Q, \mathcal{L}_m)$ gravity focussed on the study of cosmological dynamics of the universe on the background expansion history [48] and other works considered perturbation part in the context of $f(Q)$ gravity [62]. To our knowledge, there is no work in the literature on large scale structure formation scenario and matter power spectrum within the framework of $f(Q, \mathcal{L}_m)$ gravity for two different considered models in this work. We therefore fill this gap by studying the energy density perturbation and matter power spectrum of these models using the 1 + 3 covariant formalism. To

do so, we first define the covariant and gauge-invariant gradient variables that describe perturbation in the matter density, expansion, the nonmetricity scalar and its energy momentum as [62, 72]

$$D_a^m = \frac{a\tilde{\nabla}_a\rho}{\rho}, Z_a = a\tilde{\nabla}_a\theta, C_a = a\tilde{\nabla}_aQ, F_a = a\tilde{\nabla}_a(\dot{Q}) \quad (47)$$

The terms D_a^m and Z_a represent the energy density and the volume expansion of the fluid, respectively, and they are the basic tools to extract the evolution equations for matter fluctuations. Based on nonmetricity fluid, the terms C_a and F_a represent the spatial gradients of gauge-invariant quantities characterising the fluctuations in the nonmetricity density and momentum, respectively. By applying the technic commonly used in the 1+3 covariant formalism to derive the perturbation equations [62, 67], the first order evolution equations derived from eq. (47) are presented as

$$\dot{D}_a^m = -\gamma Z_a + 3(\gamma - 1)HD_a^m, \quad (48)$$

$$\dot{Z}_a = a\tilde{\nabla}_a\theta + \frac{1-\gamma}{\gamma}\dot{\theta}D_a^m, \quad (49)$$

$$\dot{C}_a = F_a + \frac{(1-\gamma)\dot{Q}}{\gamma}D_a^m, \quad (50)$$

$$\dot{F}_a = \frac{\ddot{Q}}{\dot{Q}}C_a + \frac{(1-\gamma)\ddot{Q}}{\gamma}D_a^m. \quad (51)$$

Eq. (48)–(51) are general evolution equations in the context of $f(Q, \mathcal{L}_m)$ gravity. In order to investigate the effect of the models A and B on the large scale structure formation, we need to apply each model to these perturbation equations then find the corresponding numerical results. Using eq. (11), eq. (12) and eq. (15) of the model A, the perturbation equations become

$$\dot{D}_a^m = -\gamma Z_a + 3(\gamma - 1)HD_a^m, \quad (52)$$

$$\dot{Z}_a = -3\gamma HZ_a + (1-\gamma)\left[\frac{9}{2}H^2 + \frac{3\beta}{4\alpha}\right]D_a^m, \quad (53)$$

$$\dot{C}_a = F_a + \frac{(1-\gamma)\dot{Q}}{\gamma}D_a^m, \quad (54)$$

$$\dot{F}_a = \frac{\ddot{Q}}{\dot{Q}}C_a + \frac{(1-\gamma)\ddot{Q}}{\gamma}D_a^m, \quad (55)$$

where we have used $\dot{\theta} = -\frac{9\gamma H^2}{2} + \frac{3\gamma\beta}{4\alpha}$. Eq. (52)–(55) are general perturbation equations in the context of $f(Q, \mathcal{L}_m)$ for model A. Only scalar components of the perturbation equations are believed to enhance most of large scale structure formation mechanism. Using scalar decomposition technique explored in [], and applying the time derivative on Eq. (52)–(55), we therefore have the second order ordinary differential equations responsible

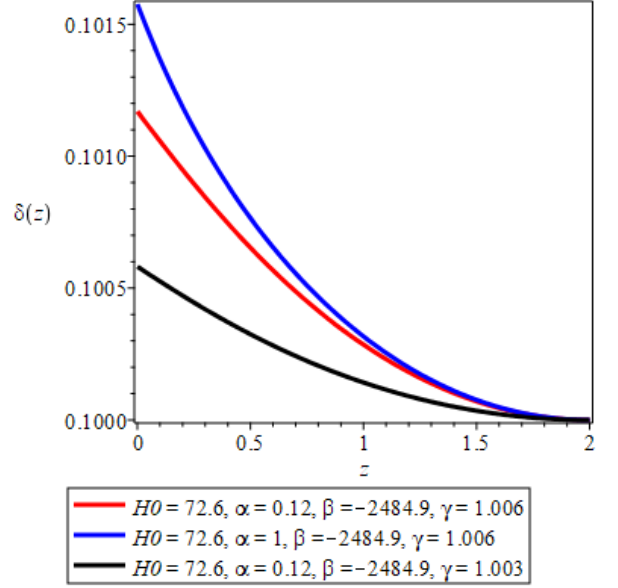


FIG. 1. Plot of energy density contrast (δ) versus redshift (z) for different values of constant parameters of Eq. (58) and eq. (59) of model A in the context of $f(Q, \mathcal{L}_m)$ gravity. The choice of values of model parameters was done basing on the constrained parameters obtained in the work done in [48]

for structure formation presented as

$$\ddot{\Delta}_m = -3H\dot{\Delta}_m + \gamma(\gamma - 1)\left[\frac{3\beta}{2\alpha} + 9H^2\right]\Delta_m, \quad (56)$$

$$\ddot{C} = \frac{\ddot{Q}}{\dot{Q}}C + \frac{2(1-\gamma)}{\gamma}\ddot{Q}\Delta_m + \dot{Q}\frac{(1-\gamma)}{\gamma}\dot{\Delta}_m. \quad (57)$$

The energy density resulting from the nonmetricity scalar (eq. (57)) couples with the matter energy density. In order to solve eq. (56) and eq. (57), let us first apply the redshift transformation technique considered in different works [62, 67, 71] presented as $a = \frac{1}{1+z}$, $\dot{f} = -(1+z)Hf'$ and $\ddot{f} = (1+z)^2H[H'f' + Hf'']$, where f' is the derivative with respect to redshift z . The equations in redshift space, when solved, help to compare the results with observations. The resulting equations are presented as

$$(1+z)^2H^2\Delta_m'' = -(1+z)H\left[(1+z)H' - 2H\right]\Delta_m' + \gamma(\gamma - 1)\left[\frac{3\beta}{2\alpha} + 9H^2\right]\Delta_m, \quad (58)$$

$$(1+z)^2H^2C'' = -(1+z)H\left[(1+z)H' + H\right]C' + \frac{l_3}{l_1}C + \frac{2(1-\gamma)}{\gamma}l_2\Delta_m - l_1\frac{(1-\gamma)}{\gamma}(1+z)H\Delta_m' \quad (59)$$

Eq. (58) and eq. (59) are the energy density perturbation equations responsible for large scale structure forma-

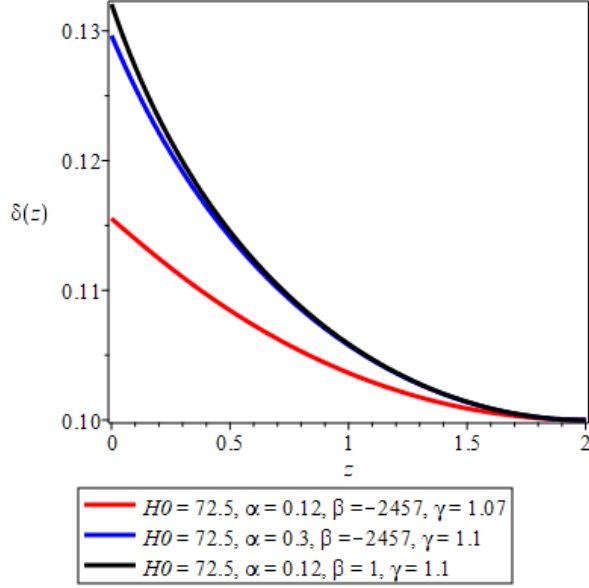


FIG. 2. Plot of energy density contrast (δ) versus redshift z for different values of constant parameters of Eq. (58) and eq. (59) of model A. The choice of values of model parameters was done basing on the constrained parameters obtained in the work done in [48] for model B

tion in the context of $f(Q, \mathcal{L}_m)$ gravity, where l_1 , l_2 and l_3 represent the first, second and third derivatives with redshift of the nonmetricity scalar. Solving the obtained equations, we need to define the energy density contrast $\delta(z) = \frac{\Delta(z)}{\Delta(z=z_{in})}$, where z_{in} is the initial redshift. We also define the initial conditions of the energy densities as $\Delta'(z = z_{in} = 0)$, $\Delta(z = z_{in} = 10^{-5})$, $C'(z = z_{in} = 0)$, $C(z = z_{in} = 10^{-5})$. By varying the model parameters, numerical results of Eq. (58) and eq. (59) are presented in Fig. (1) and Fig. (2). But looking at the figures, the energy density contrast decays as the redshift increases, which implies the perturbation amplitudes are higher in the present universe ($z = 0$).

By going through the same procedures used to obtain the perturbation equations for model A, we can also obtain the perturbation equations for model B. Using Eqs. (48)–(51), eqs. (30)–(32) together with $\dot{\theta} = -\frac{9\gamma H^2}{\gamma+1} - \frac{3\gamma\beta}{2\alpha(\gamma+1)}$, the energy density perturbation equations for model B, in redshift space in the context of

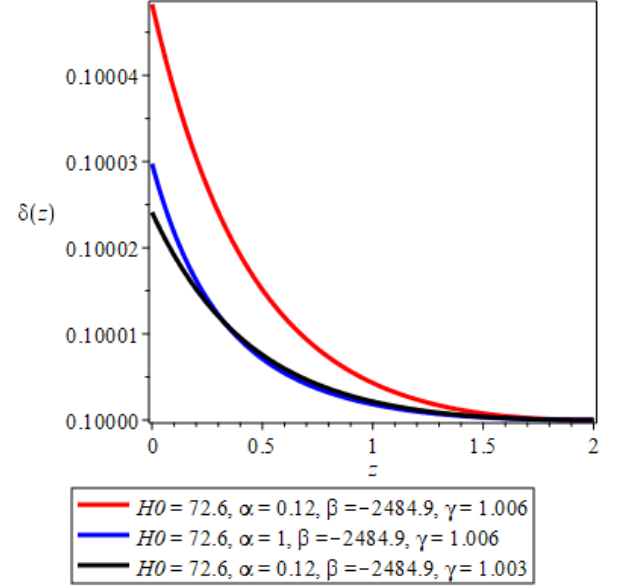


FIG. 3. Plot of energy density contrast (δ) versus redshift z for different values of constant parameters of eq. (61) and eq. (61) of model B in the context of $f(Q, \mathcal{L}_m)$ gravity.

$f(G, \mathcal{L}_m)$ gravity, are given by

$$\begin{aligned} (1+z)^2 H^2 \Delta_m'' &= -(1+z) H \left[(1+z) H' \right. \\ &\quad \left. + H \left(3\gamma - 2 - \frac{6\gamma}{\gamma+1} \right) \right] \Delta_m' + \frac{3\gamma(1-\gamma)}{\gamma+1} [1+\beta] \Delta_m \\ (1+z)^2 H^2 C'' &= -(1+z) H \left[(1+z) H' + H \right] C' + \\ &\quad \frac{l_3}{l_1} C + \frac{2(1-\gamma)}{\gamma} l_2 \Delta_m - l_1 \frac{(1-\gamma)}{\gamma} (1+z) H \Delta_m' \end{aligned} \quad (61)$$

The numerical results of eq. (61) and eq. (61) are presented in Fig. (3) and Fig. (4) obtained by interchanging the model parameters. Looking at the plots, the energy density contrast decays with redshift.

After obtaining the energy density perturbation equations and their corresponding numerical results and finding that the energy density contrasts decay with redshift for both models, next step is to investigate the implications of the considered models on the matter power spectrum.

IV. MATTER POWER SPECTRUM IN $f(Q, \mathcal{L}_m)$ GRAVITY

In order to get the matter power spectrum for each model, we first put the autonomous dynamical system equations for model A (eq. (26)–(29)) into eq. (58) and eq. (59) to get the normalised perturbation equations for

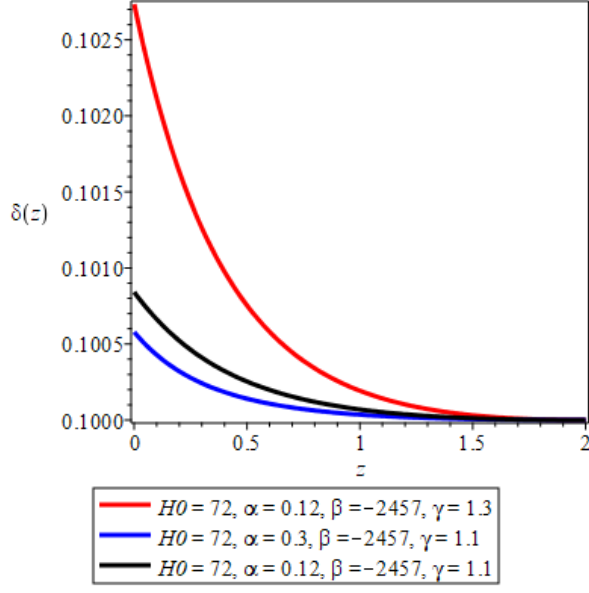


FIG. 4. Plot of energy density contrast δ versus redshift z for different values of constant parameters of eq. (61) and eq. (61) of model B in the context of $f(Q, \mathcal{L}_m)$ gravity.

model A given by

$$\Delta_m'' = -\frac{1}{(1+z)} \left[\frac{3\gamma(1+x)}{2} - 2 \right] \Delta_m' + 9 \frac{\gamma(\gamma-1)}{(1+z)^2} (x+1) \Delta_m, \quad (62)$$

$$\mathcal{C}'' = -\frac{1}{(1+z)} \left[\frac{3\gamma(1+x)}{2} + 1 \right] \mathcal{C}' + \frac{\beta l_3}{6(1+z)^2 \alpha x l_1} \mathcal{C} + \frac{\beta(1-\gamma)}{3(1+z)^2 \alpha x \gamma} l_2 \Delta_m - l_1 \frac{(1-\gamma)}{\gamma(1+z)} \left(\frac{\beta}{6\alpha x} \right)^{\frac{1}{2}} \Delta_m' \quad (63)$$

By assuming an isotropic FRW universe, the matter power spectrum in the context of $f(Q, \mathcal{L}_m)$ gravity, which can be compared to the Λ CDM predictions at any given scale k can be represented as [54–56]

$$P^{f(Q, \mathcal{L}_m)}_k = (|\Delta(k)|)^2.$$

Put the autonomous dynamical system equations for model B (eq. (43)–(46)) into the perturbation equations eq. (61) and eq. (61) to get normalised perturbation equations for model B presented as

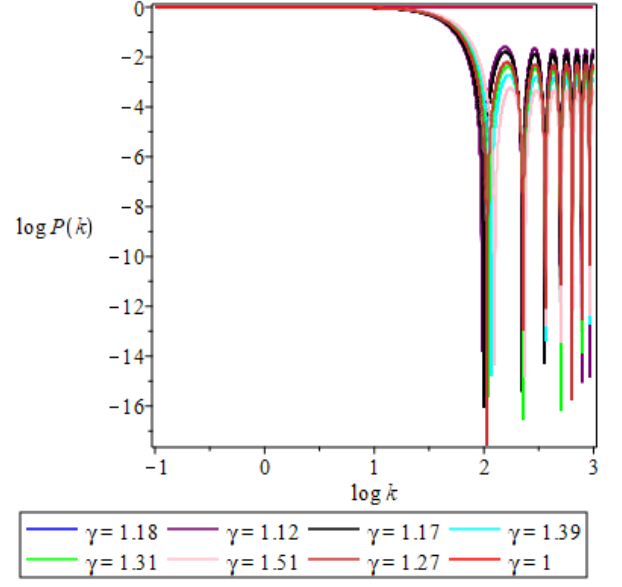


FIG. 5. Plot matter power spectra for different values of γ for $\alpha = 0.3$ and $\beta = -0.0001$ of eq. (62) and eq. (63) of model A in the context of $f(Q, \mathcal{L}_m)$ gravity. We use the initial conditions $\Delta(z) = 10^{-5}$, $\Delta'(z) = 0$, $\mathcal{C}(z) = 10^{-5}$, $\mathcal{C}'(z) = 0$.

$$\Delta_m'' = -\frac{1}{(1+z)} \left[\frac{3(1+y)}{1+\gamma} + \left(3\gamma - 2 - \frac{6\gamma}{\gamma+1} \right) \right] \Delta_m' + \frac{3\gamma(1-\gamma)}{\gamma+1} [1+\beta] \Delta_m, \quad (64)$$

$$\mathcal{C}'' = -\frac{1}{(1+z)} \left[\frac{3(1+y)}{1+\gamma} + 1 \right] \mathcal{C}' + \frac{\beta l_3}{6(1+z)^2 \alpha y l_1} \mathcal{C} + \frac{\beta(1-\gamma)}{3(1+z)^2 \alpha y \gamma} l_2 \Delta_m - l_1 \frac{(1-\gamma)}{\gamma(1+z)} \left(\frac{\beta}{6\alpha y} \right)^{\frac{1}{2}} \Delta_m' \quad (65)$$

In order to compute the matter spectra for each model, we consider 3 different sets of initial conditions for the system of equations eq. (62) and eq. (63) for model A and eq. (64) and eq. (65) for model B, in order to interpret the sensitivity of the models on the matter spectra. To obtain the numerical results, for model A, we solve simultaneously eq. (26)–eq. (29) to get redshift-dependent solutions for parameters x , Ω_1 and Ω_2 . We then use the obtained solutions together with the solutions of eq. (62) and eq. (63) to get the matter power spectra for model A. The power spectra for model A are presented in Fig. (5) and Fig. (6). For model B, we solve eq. (43)–eq. (46) to obtain redshift-dependent solutions for the parameters y , Ω_3 and Ω_4 . Using these solutions together with the solutions of eq. (64) and eq. (65), we compute the matter power spectra for model B. The power spectra for model

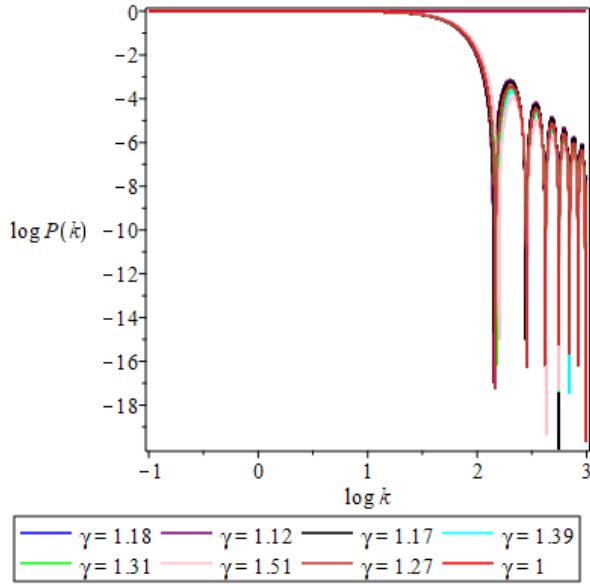


FIG. 6. Plot matter power spectra for different values of γ for $\alpha = 0.3$ and $\beta = -0.0001$ of eq. (62) and eq. (63) of model A in the context of $f(Q, \mathcal{L}_m)$ gravity. We use the initial conditions $\Delta(z) = 10^{-5}$, $\Delta'(z) = 10^{-3}$, $\mathcal{C}(z) = 10^{-5}$, $\mathcal{C}'(z) = 10^{-3}$.

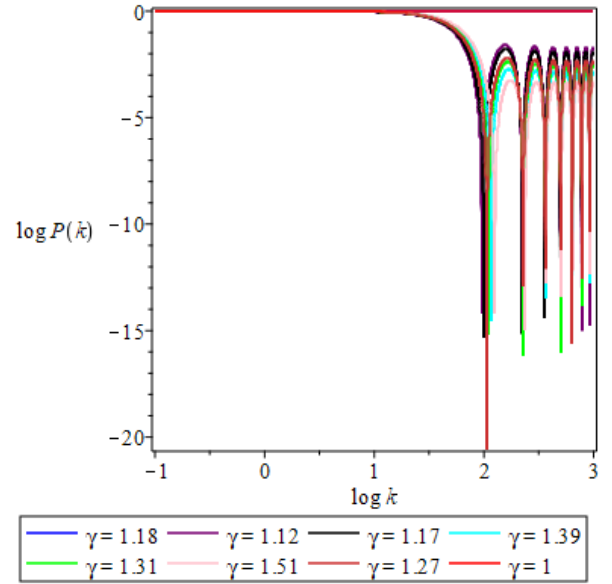


FIG. 7. Plot matter power spectra for different values of γ for $\alpha = 0.3$ and $\beta = -0.0001$ of eq. (62) and eq. (63) of model A in the context of $f(Q, \mathcal{L}_m)$ gravity. We use the initial conditions $\Delta(z) = 10^{-5}$, $\Delta'(z) = 10^{-8}$, $\mathcal{C}(z) = 10^{-5}$, $\mathcal{C}'(z) = 10^{-8}$.

B are presented in Fig. (7) and Fig. (8).

V. STRUCTURE GROWTH AND DATA ANALYSIS

In this section, it is worth to extend the analysis of the perturbation equations and its role on structure formation to observational context. In doing so, we first derive a structure growth equation, then use different observational data sets to discuss the compatibility of the models with observation. Let us first seek the growth equation in the following subsection.

A. Structure growth equation in the context of $f(Q, \mathcal{L}_m)$ gravity

To constrain the matter energy density fluctuations with observations, we consider the redshift-space distortions (RSD) discussed mainly in [57–60]. Following these works, we compute the combinations $f\sigma_8$ in the context of $f(Q, \mathcal{L}_m)$ gravity. We first present the linear growth rate f as

$$f = -(1+z) \frac{\Delta'_m(z)}{\Delta_m(z_{in})}, \quad (66)$$

and using eq. (66), together with the quasi-static approximation [62], eqs. (58) and (59) can be related to

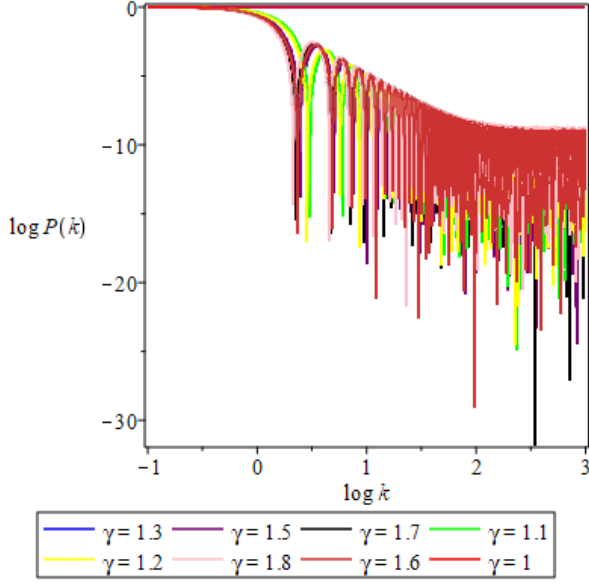


FIG. 8. Plot matter power spectra for different values of γ for $\alpha = 0.4$ and $\beta = -0.0001$ of eq. (64) and eq. (65) of model B in the context of $f(Q, \mathcal{L}_m)$ gravity. We use the initial conditions $\Delta(z) = 10^{-5}$, $\Delta'(z) = 10^{-3}$, $\mathcal{C}(z) = 10^{-5}$, $\mathcal{C}'(z) = 10^{-3}$.

the linear growth rate as

$$\begin{aligned} (1+z)f' = -f^2 - \left[(1+z)\frac{E'}{E} - 3\right]f - 9\gamma(\gamma-1) \\ - \frac{3\gamma(\gamma-1)\beta}{2\alpha H_0^2 E^2}, \end{aligned} \quad (67)$$

where $E^2 = \frac{H^2}{H_0^2}$ is obtained from eq. (11) as

$$E^2 - \frac{1}{\alpha} \left[\Omega_m (1+z)^3 + \frac{\beta}{12H_0^2} \right] = \Omega_m (1+z)^3. \quad (68)$$

Solving eq. (67) numerically for $f(z)$ and combining $f(z)$ with σ_8 , where σ_8 is the root mean square normalisations of the matter power spectrum within the radius sphere of $8h^{-1} \text{MPC}$ [62] defined as

$$\sigma_8(z) = \sigma_8(z_{in}) \frac{\Delta_m(z)}{\Delta_m(z_{in})}, \quad (69)$$

the combination $f\sigma_8(z)$ can be presented as [57, 59–62]

$$f\sigma_8(z) = -(1+z)\sigma_8(z) \frac{\Delta'_m(z)}{\Delta_m(z_{in})}. \quad (70)$$

Eq. (67) and Eq. (70) will be used to confront the model parameters with the RSD data set using MCMC. The values $\delta'_m(z)$, $\delta_m(z)$ and $\delta_m(z_{in})$ are obtained by solving numerically eqs. (58) and (59) for a given set of initial conditions. This theoretical results can now be used to constrain the parameters (Ω_m , σ_8 , γ , H_0 , α and β) using $f\sigma_8$ data in the context of $f(G)$ gravity model. In the

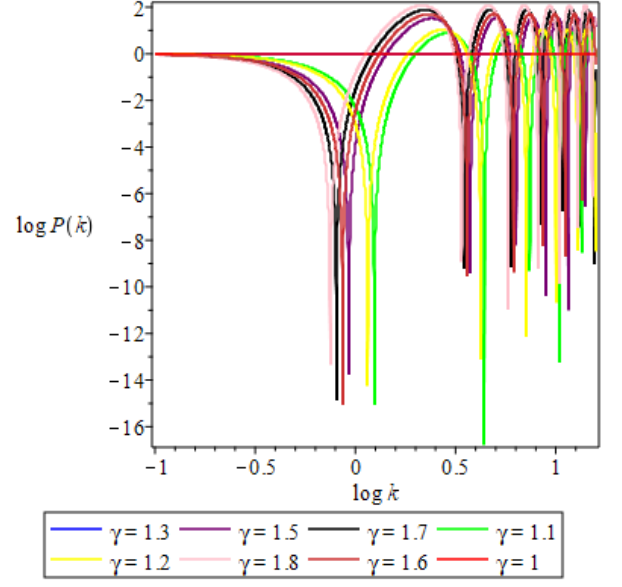


FIG. 9. Plot matter power spectra for different values of γ for $\alpha = 0.4$ and $\beta = -0.0001$ of eq. (64) and eq. (65) of model B in the context of $f(Q, \mathcal{L}_m)$ gravity. We use the initial conditions $\Delta(z) = 10^{-5}$, $\Delta'(z) = 10^{-8}$, $\mathcal{C}(z) = 10^{-5}$, $\mathcal{C}'(z) = 10^{-8}$.

next section, we introduce different observational data sets to be considered to compare our $f(Q, \mathbf{L}_m)$ gravity model with observation using MCMC.

VI. DATA ANALYSIS AND RESULTS

In this section, we discuss and present the observational data used to constrain the model parameters using the MCMC analysis.

A. Data analysis

- **CC Data:** This data set contains 32 model-independent observational points corresponding to the Hubble parameter, commonly referred to as Cosmic Chronometers (CC) [74, 75].
- **PP Data:** This data set consists of 1550 spectroscopically confirmed Type Ia supernovae [76]. The full catalog contains 1770 data samples, from which we use the observational column corresponding to the non-SH0ES-calibrated apparent magnitude m_{obs} . We refer to this data set as ‘PP’.
- **DES Data:** This data set contains Type Ia Supernovae samples from a different observation – the Dark Energy Survey (DES-SN5YR) – which includes 1829 distinct SNe [77, 78]. It consists of 194 nearby SNe samples with redshift $0 < z < 0.1$ and

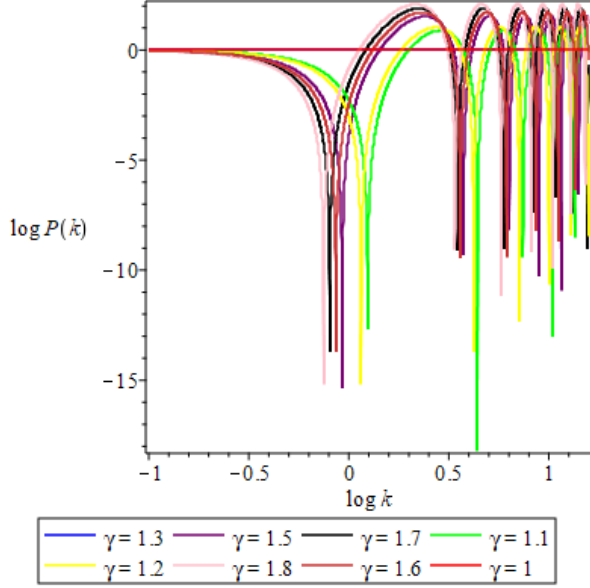


FIG. 10. Plot matter power spectra for different values of γ for $\alpha = 0.4$ and $\beta = -0.0001$ of eq. (64) and eq. (65) of model B in the context of $f(Q, \mathcal{L}_m)$ gravity. We use the initial conditions $\Delta(z) = 10^{-5}$, $\Delta'(z) = 0$, $\mathcal{C}(z) = 10^{-5}$, $\mathcal{C}'(z) = 0$.

1635 DES SNe samples. The catalog provides the distance modulus μ along with the full covariance matrix. The distance modulus is defined as:

$$\mu \equiv m - M_b = 5 \log(D_L/\text{Mpc}) + 25, \quad (71)$$

where, m denotes the apparent magnitude of the supernova, M_b is the absolute magnitude and D_L is the luminosity distance:

$$D_L(z) = c(1+z) \int_0^z \frac{dz'}{H(z')}, \quad (72)$$

assuming a flat FLRW metric, and c is the speed of light in km/s. The model parameters are constrained by minimizing the chi-square (χ^2) likelihood, defined as:

$$-2 \ln(\mathcal{L}) = \chi^2 = \Delta \mathbf{D}_i \mathcal{C}_{ij}^{-1} \Delta \mathbf{D}_j, \quad (73)$$

where $\Delta \mathbf{D} = \mu_{\text{Obs}} - \mu_{\text{Model}}$. We label this data set as ‘DES’.

- **DESI BAO:** This data set includes samples of Baryon Acoustic Oscillations (BAO) from the Dark Energy Spectroscopic Instrument (DESI) Release II [79]. The observables are $\{D_M/r_d, D_H/r_d, D_V/r_d\}$, where D_M denotes the comoving angular diameter distance, D_H the Hubble distance, D_V the spherically averaged distance, and r_d the sound horizon at the drag epoch, corresponding to the redshift $z_d = 1060.0$ [80–82],

$$r_d = \int_{z_d}^{\infty} \frac{3 \times 10^5 dz}{H \sqrt{3 \left(1 + \frac{3\Omega_{b0} h^2}{4\Omega_{\gamma0} h^2 (1+z)} \right)}}. \quad (74)$$

Model A	
Parameters	Range
H_0	[30, 100]
α	[0, 0.5]
β	[-4000, -1000]
γ	[1.0, 2.0]
r_d	[100, 300]
σ_8	[0, 0.9]
M_b	[-20.0, -18.0]

TABLE I. The uniform prior range on the model parameters.

Here, $\Omega_{\gamma0} h^2$ denotes the photon density parameter and $h \equiv H_0/100$, with the value 2.472×10^{-5} and Ω_{b0} represents the baryon density at the present epoch with the value $\Omega_{b0} h^2 = 0.02236$ [82, 83]. However, for this study we will treat r_d as a free parameter. We refer to this data set as ‘BAO’.

- **$f\sigma_8$ Data :** This data sets includes 30 observational samples of redshift-space distortion $f\sigma_8$ in the redshift $z \in [0.001, 1.944]$ [62]. We label this data set as ‘fs8’.

For the above data sets, we compute the joint likelihood corresponding to following combinations of datasets: (i) CC+PP (ii) CC+DES (iii) CC+BAO+fs8 (iv) CC+BAO+fs8+PP (v) CC+BAO+fs8+DES. The joined likelihood is estimated as

$$-2 \ln \mathcal{L}_{\text{tot}} = \chi_{\text{tot}}^2. \quad (75)$$

The likelihood is estimated by implementing the model in **Python** using the publicly available affine-invariant Markov Chain Monte Carlo (MCMC) ensemble sampler **emcee** [84]. The resulting posterior distributions are visualized using triangular (corner) plots, generated by analyzing the MCMC chains with **GetDist** [85].

B. Results

In this section, we present the parameter estimation for Model A by varying the free parameters associated with the Hubble parameter (see Eq. (15)), alongside other key cosmological quantities—namely, the absolute magnitude of Type Ia supernovae M_b , the sound horizon at the end of the drag epoch r_d , and the root-mean-square normalization of the matter power spectrum σ_8 , defined within a sphere of radius $8h^{-1}$ Mpc. A uniform prior is adopted for each parameter as summarized in Tab. (I).

We begin by testing the flat Λ CDM model as a baseline, varying H_0 and Ω_{m0} over the ranges [30, 100] and [0, 0.8], respectively. The resulting posterior distributions, marginalized over M_b , are shown in Fig. (11), and the best-fit values are presented in Tabs. (II) and (III). Model A is tested using two separate Type Ia supernova catalogs, each yielding distinct values of H_0 as seen in

CC+PP- Λ CDM CC+DES- Λ CDM		
Parameter	68% limits	68% limits
H_0	67.0 ± 1.8	69.07 ± 0.28
Ω_m	0.358 ± 0.018	0.357 ± 0.011
M_b	-19.436 ± 0.057	—

CC+PP-Model A CC+DES-Model A		
Parameters	68% limits	68% limits
H_0	66.8 ± 1.8	69.08 ± 0.28
α	0.144 ± 0.019	0.133 ± 0.016
β	-2530^{+210}_{-430}	-2510 ± 290
γ	$1.0292^{+0.0064}_{-0.029}$	$1.0265^{+0.0060}_{-0.027}$
M_b	-19.445 ± 0.056	—

TABLE II. The model parameter's best fit values obtained from MCMC.

Tab. (II), indicating tension between the datasets. However, the other cosmological parameters remain in good agreement. The recovered values of H_0 are consistent with those from Λ CDM, suggesting that the discrepancy arises primarily due to differences in calibration between the datasets.

For the Pantheon+ (PP) dataset, H_0 and M_b exhibit strong degeneracy. To break this, we include external Cosmic Chronometer (CC) data, resulting in a value of $H_0 \approx 67.0$ km/s/Mpc—closely matching the Planck Collaboration's result [82]. In contrast, the DES catalog provides a calibrated distance modulus μ , leading to $H_0 \approx 69.08$ km/s/Mpc—closer to the SH0ES result [76]. We further extend the analysis by including BAO and $f\sigma_8$ datasets and re-evaluating both Model A and Λ CDM. The corresponding best-fit values are listed in Tab. (III), and the posterior distributions are shown in Fig. (11). The inclusion of these datasets brings all three combinations to a consistent $H_0 \sim 69.6$ km/s/Mpc. The values of $\sigma_8 \sim 0.761$ and $r_d \sim 145.0$ Mpc remain nearly unchanged across datasets for flat Λ CDM.

When Model A is tested with the $f\sigma_8$ datasets, the posterior distributions shown in Fig. (12) and the best-fit parameters in Tab. (III) indicate $H_0 \sim 70.0$ km/s/Mpc for both CC+BAO+fs8+PP and CC+BAO+fs8+DES combinations—slightly higher than the corresponding Λ CDM result. The effective equation of state parameter γ for the background fluid is found to be $\gamma \sim 1.07$ for both combinations, indicating a mild deviation from pressure-less dark matter ($\gamma = 1$). A similar value is also obtained for CC+PP and CC+DES data sets ($\gamma \sim 1.03$). The derived values of r_d and M_b remain consistent with Λ CDM, though σ_8 shows noticeable deviation.

Specifically, the DES dataset yields $\sigma_8 \sim 0.66$ for Model A, which deviates from Λ CDM by about 2.2σ . This suggests a potential resolution to the σ_8 tension in this context. Using the CC+BAO+fs8 combination alone, Model A yields $H_0 \sim 72.3$ km/s/Mpc—very close to the SH0ES value. However, in this case, $\gamma \sim 1.12$, in-

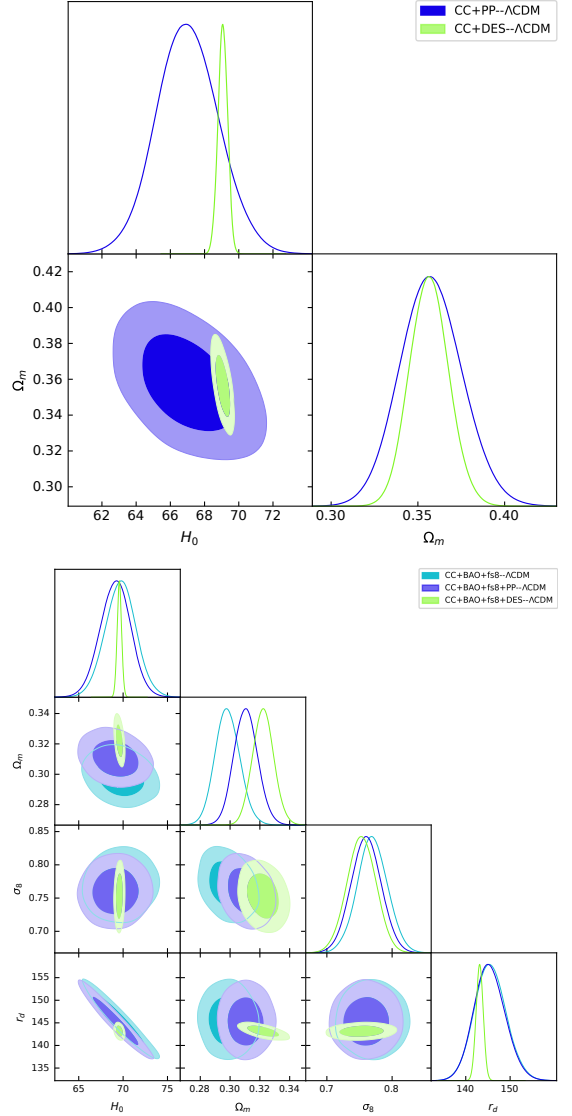


FIG. 11. The 1D 2D marginalized parameter distribution for Λ CDM marginalizing M_b .

dicating a significant deviation from a pressure-less fluid. Despite this, σ_8 and r_d remain compatible with Λ CDM values.

In summary, while Model A can yield a higher H_0 , consistent with local measurements, the inclusion of larger and more diverse datasets tends to pull the model closer to the Λ CDM values, limiting its ability to fully resolve the Hubble tension. Nonetheless, it offers a compelling and physically viable alternative to the standard cosmological model.

VII. DISCUSSIONS AND CONCLUSION

In this study, we explored the energy density perturbations and matter power spectrum within the frame-

TABLE III. The parameter's best fit values obtained from MCMC. The dashed shows that the corresponding parameter is not fitted for that particular data set.

	CC+BAO+fs8+PP- Λ CDM	CC+BAO+fs8+DES- Λ CDM	CC+BAO+fs8- Λ CDM
Parameter	68% limits	68% limits	68% limits
H_0	69.1 ± 1.7	69.58 ± 0.25	69.7 ± 1.7
Ω_m	0.3106 ± 0.0079	0.3222 ± 0.0071	0.2983 ± 0.0083
σ_8	0.760 ± 0.023	0.753 ± 0.022	0.770 ± 0.023
r_d	$145.4^{+3.3}_{-3.7}$	143.13 ± 0.80	145.5 ± 3.6
M_b	-19.384 ± 0.053	–	–
<hr/>			
	CC+BAO+fs8+PP-Model A	CC+BAO+fs8+DES-Model A	CC+BAO+fs8-Model A
Parameter	68% limits	68% limits	68% limits
H_0	70.4 ± 1.8	69.87 ± 0.28	72.3 ± 1.8
α	$0.117^{+0.052}_{-0.034}$	$0.133^{+0.054}_{-0.025}$	$0.108^{+0.042}_{-0.026}$
β	-2650^{+650}_{-1300}	-2790^{+460}_{-1200}	-2760^{+510}_{-1100}
γ	$1.087^{+0.015}_{-0.013}$	1.050 ± 0.016	1.127 ± 0.013
σ_8	0.711 ± 0.034	0.656 ± 0.038	0.751 ± 0.029
r_d	145.1 ± 3.5	142.99 ± 0.81	$145.4^{+3.3}_{-3.7}$
M_b	-19.359 ± 0.054	–	–

work of $f(Q, \mathcal{L}_m)$ gravity, where Q represents the non-metricity scalar and \mathcal{L}_m denotes the matter Lagrangian. We used two different cosmological models namely model A and model B defined as $f = -\alpha Q + 2l_m + \beta$ and $f = -\alpha Q + (2l_m)^2 + \beta$ respectively, to analyse their effects on perturbation levels and on the matter power spectrum in the context of $f(Q, \mathcal{L}_m)$ gravity, where α and β are model parameters. Using dynamical system analysis, we obtain the autonomous ordinary differential equations for each models, namely eq. (26)–(29) and eq. (43)–(46). These autonomous equations are helpful in computing matter power spectrum. Defining gradient variables responsible for large scale structure formation and using scalar decomposition, harmonic decomposition together with redshift transformation techniques, we derive and present the energy density perturbation equation in redshift space (eq. (58)–(59) for model A and eq. (61)–(61) for model B) using the 1 + 3 covariant formalism. These perturbation equations are believe to enhance matter clustering, hence responsible for structure formation. Using different initial conditions such as $\Delta(z_{in}) = 10^{-5}$, $\Delta'(z_{in}) = 0$, $\mathcal{C}(z_{in}) = 10^{-5}$ and $\mathcal{C}'(z_{in}) = 0$ and defining the energy density contrast as $\delta(z) = \frac{\Delta(z)}{\Delta(z_{in})}$, we solve numerically the perturbation equations for both models and the results are presented in Fig. (1) and Fig. (2) for model A, whereas Fig. (3) and Fig. (4) represent numerical results for model B. For model A, the energy density contrast decays with redshift. By changing the model parameters such as α and γ , the amplitudes of the $\delta(z)$ change significantly as can be shown in Fig. (1) and Fig. (2). By looking at Fig. (3) and Fig. (4) of model B, the energy density contrast ($\delta(z)$) decays with red-

shift and the amplitudes are affected by changing model parameters. For both models, the $\delta(z)$ decays with redshift but dies off quickly for model B than model A as the redshift increases. After solving numerically the perturbation equations for both models and obtaining the density contrast, we use the obtained autonomous ordinary differential equations (eq. (26)–(29)) together with the perturbation equations eq. (58)–(59) for model A to compute matter power spectra in the context of $f(Q, \mathcal{L}_m)$ gravity. The matter power spectra are presented in Fig. (5) using $\Delta(z_{in}) = 10^{-5}$, $\Delta'(z_{in}) = 0$, $\mathcal{C}(z_{in}) = 10^{-5}$ and $\mathcal{C}'(z_{in}) = 0$ as initial conditions, in Fig. (6) using $\Delta(z_{in}) = 10^{-5}$, $\Delta'(z_{in}) = 10^{-3}$, $\mathcal{C}(z_{in}) = 10^{-5}$ and $\mathcal{C}'(z_{in}) = 10^{-3}$ as initial conditions and in Fig. (7) using $\Delta(z_{in}) = 10^{-5}$, $\Delta'(z_{in}) = 10^{-8}$, $\mathcal{C}(z_{in}) = 10^{-5}$ and $\mathcal{C}'(z_{in}) = 10^{-8}$ as initial conditions. Furthermore, using the obtained autonomous ordinary differential equations (eq. (43)–(46)) together with the perturbation equations eq. (61)–(61 for model B, we compute matter power spectra in the context of $f(Q, \mathcal{L}_m)$ gravity. The matter power spectra are presented in Fig. (8) using $\Delta(z_{in}) = 10^{-5}$, $\Delta'(z_{in}) = 10^{-3}$, $\mathcal{C}(z_{in}) = 10^{-5}$ and $\mathcal{C}'(z_{in}) = 10^{-3}$ as initial conditions, in Fig. (9) using $\Delta(z_{in}) = 10^{-5}$, $\Delta'(z_{in}) = 10^{-8}$, $\mathcal{C}(z_{in}) = 10^{-5}$ and $\mathcal{C}'(z_{in}) = 10^{-8}$ as initial conditions and in Fig. (10) using $\Delta(z_{in}) = 10^{-5}$, $\Delta'(z_{in}) = 0$, $\mathcal{C}(z_{in}) = 10^{-5}$ and $\mathcal{C}'(z_{in}) = 0$ as initial conditions. By looking at all matter power spectra for both models, the curves decay and remain under the General Relativity (GR) scale invariant line as k increase for model A, whereas the curves decay and evolve above the GR invariant line for model B. As the initial conditions changes, there appear a slight changes in the behaviour of the matter power spectra curves. In the present work,

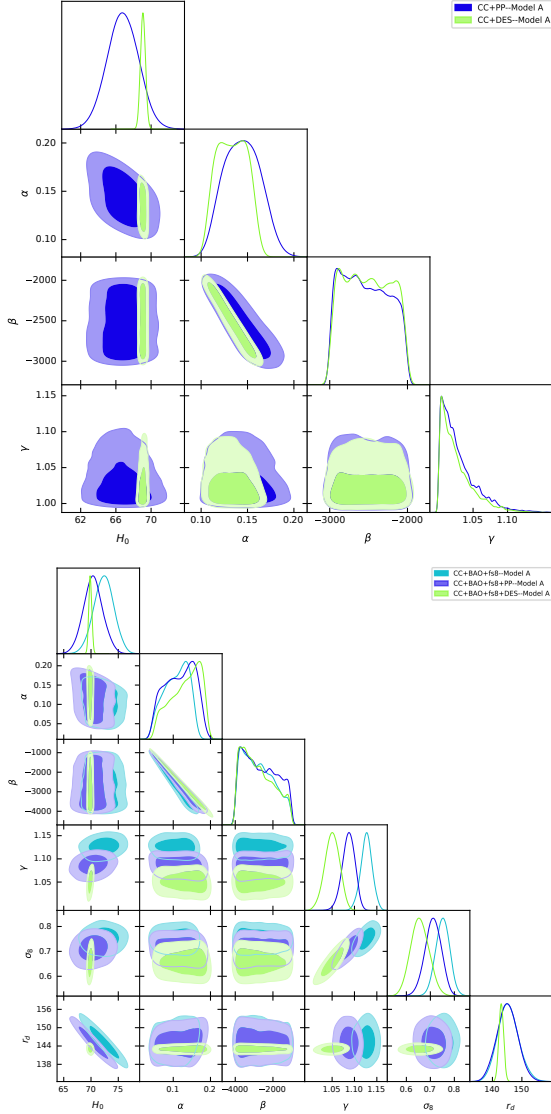


FIG. 12. The posterior distribution for Model A marginalizing M_b .

one can highlight that

- The obtained matter contrasts $\Delta(z)$ couple with the the density contrast resulting from the $f(Q, \mathcal{L}_m)$ models $\mathcal{C}(z)$, therefore $\mathcal{C}(z)$ influences the behavior of both energy density contrasts and matter power spectra for both models.
- The obtained density contrasts $\delta(z)$ decay with redshift for both models
- The obtained matter power spectra decay with a change in amplitude and remain below GR invariant line for model A and evolve above GR invariant line for model B as k increases for different values of γ and initial conditions.
- For all sets of initial conditions, there was no oscil-

lations behaviour pictured as identified in the work carried out by [56, 86]. These results agree with those obtained in [87].

Motivated by the positive feedback of the considered models in the context of $f(Q, \mathcal{L}_m)$ gravity, since the models present significant results at the perturbation level, we further analyse the implications of the considered models observationally, we use different observational datasets and MCMC analysis to constrain the model parameters. Using (i) CC+PP (ii) CC+DES (iii) CC+BAO+fs8 (iv) CC+BAO+fs8+PP (v) CC+BAO+fs8+DES, the resulting posterior distributions are visualized using triangular (corner) plots, generated by analysing the MCMC chains with **GetDist**. The marginalized parameter distribution is shown in Fig. (11) and the corresponding best fit values are given in Tab. [II], respectively for (i) CC+PP (ii) CC+DES. This table contains the mean values and corresponding errors. For this particular form of $f(Q, \mathcal{L}_m)$ gravity model, we found that for the pantheon data set including the CC data, $H_0 = 66.8 \text{ km/s/MPC}$ —closely matching the plank collaboration results. Using two separate type I_a Supernova, we recover H_0 value consistent with those from ΛCDM . The DES catalogue provides $H_0 = 69.08 \text{ km/s/MPC}$ closer to the SHOES results. We notice that our findings are quite similar to the results reported in [62, 88] and [89] for different gravity models considered. After constraining the model parameters resulting from the modified Friedmann equation for the background, we extend our analysis to the perturbation level and we find the structure growth equation (eq. 67). This equation combined with σ_8 (eq. 70) enables us to constrain model parameters including σ_8 . The obtained mean values and corresponding errors are presented in table (III) and the corner plot for RSD data is presented in fig. (12). For the ΛCDM , we found that for the BAO and RSD data sets, $H_0 = 69.6 \text{ km/s/MPC}$ and $\sigma_8 = 0.761$, whereas for this particular form of $f(Q, \mathcal{L}_m)$ gravity model $H_0 = 70.0 \text{ km/s/MPC}$ for CC+BAO+fs8+PP and CC+BAO+fs8+DES combinations—higher than ΛCDM results. The results can be put in comparison with the findings reported in [60, 62, 88, 89] and in [90] which we find no contradiction. An effective equation of state $\gamma = 1.07$ deviates from pressure-less dark matter ($\gamma = 1$) and this deviation do appear also for CC+PP and CC+DES data sets, where $\gamma = 1.03$. The obtained value of σ_8 shows noticeable deviation from the ΛCDM value. DES data set yields $\sigma_8 = 0.66$ for model A, with a deviation from ΛCDM by around 2.2σ —suggesting a potential resolution to the σ_8 tension in this $f(Q, \mathcal{L}_m)$ gravity context. CC+BAO+fs8 combination yields $H_0 = 72.3 \text{ km/s/MPC}$, very close to the SHOES value. In this case $\gamma = 1.12$ indicating a significant deviation from a pressure-less fluid. The results show that the $f(Q, \mathcal{L}_m)$ gravity fits the data well as compared with the ΛCDM parameter Values, indicating that this particular choice of $f(Q, \mathcal{L}_m) = -\alpha Q + 2l_m + \beta$ gravity model has potential to explain the dynamics of the universe including the

cosmic accelerated phase and align well with observations at perturbation level unlike for the $f = -\alpha Q + (2l_m)^2 + \beta$ model (Model B) which failed to fit the considered data sets. In conclusion, this type of phenomenology analysis of $f(Q, \mathcal{L}_m)$ gravity models provides insight on the types of deviations that might be expected on cosmological observables and that can be used to distinguish the model from Λ CDM. Therefore it will be of interest to constrain different $f(Q, \mathcal{L}_m)$ gravity models from combined data analysis of large scale structure, CMB, BAO and $SN I_a$ data sets. Work in this context is in progress.

ACKNOWLEDGMENTS

PKD would like to acknowledge the Inter-University Centre for Astronomy and Astrophysics (IUCAA), Pune, India for providing him a Visiting Associateship under which a part of this work was carried out. AM acknowledges the hospitality of the University of Rwanda-College of Science and Technology, where part of this work was conceptualised and completed. SH acknowledges the support of National Natural Science Foundation of China under Grants No. W2433018 and No. 11675143, and the National Key Research and development Program of China under Grant No. 2020YFC2201503.

-
- [1] Riess Adam G et al., *Observational evidence from supernovae for an accelerating universe and a cosmological constant*, *The astronomical journal* **116** (1998) 1009.
 - [2] Giostri R et al., *From cosmic deceleration to acceleration: new constraints from SN Ia and BAO/CMB*, *Journal of Cosmology and Astroparticle Physics* **2012** (2012) 027.
 - [3] Komatsu Eiichiro et al., *Five-year wilkinson microwave anisotropy probe* observations: cosmological interpretation*, *The Astrophysical Journal Supplement Series* **180** (2009) 330.
 - [4] Jarosik N et al., *Seven-year wilkinson microwave anisotropy probe (WMAP*) observations: Sky maps, systematic errors, and basic results*, *The Astrophysical Journal Supplement Series* **192** (2011) 14.
 - [5] Weinberg David H et al., *Observational probes of cosmic acceleration*, *Physics reports* **530** (2013) 87–255.
 - [6] Delubac Timothee et al., *Baryon acoustic oscillations in the Ly α forest of BOSS quasars* *Astronomy & Astrophysics* **552** (2013) A96.
 - [7] Daniel Scott F et al., *Large scale structure as a probe of gravitational slip*, *Physical Review D—Particles, Fields, Gravitation, and Cosmology* **77** (2008) 103513.
 - [8] Capozziello Salvatore, Stabile Arturo and Troisi A *Newtonian limit of $f(R)$ gravity*, *Physical Review D—Particles, Fields, Gravitation, and Cosmology* **76** (2007) 104019.
 - [9] Ilyas Maham and Ahmad Daud *Stability analysis of anisotropic stellar structures in $f(R)$ gravity*, *Chinese Journal of Physics* **88** (2024) 901–912.
 - [10] Sharif M and Saba Saadia *Ghost dark energy model in $f(G)$ gravity*, *Chinese Journal of Physics* **58** (2019) 202–211.
 - [11] Lohakare Santosh V, Niyogi Soumyadip and Mishra B *Cosmology in modified $f(G)$ gravity: a late-time cosmic phenomena*, *Monthly Notices of the Royal Astronomical Society* **535** (2024) 1136–1146.
 - [12] Myrzakulov Ratbay *Accelerating universe from $F(T)$ gravity*, *The European Physical Journal C* **71** (2011) 1752.
 - [13] Heisenberg Lavinia *Review on $f(Q)$ gravity*, *Physics Reports* **1066** (2024) 1–78.
 - [14] Mandal Sanjay, Sahoo PK and Santos Joao RL *Energy conditions in $f(Q)$ gravity*, *Physical Review D* **102** (2020) 024057.
 - [15] Song Yong-Seon, Hu Wayne and Sawicki Ignacy *Large scale structure of $f(R)$ gravity*, *Physical Review D—Particles, Fields, Gravitation, and Cosmology* **75** (2007) 044004.
 - [16] Böhmer Christian G, Harko Tiberiu and Lobo Francisco *SN Dark matter as a geometric effect in $f(R)$ gravity*, *Astroparticle Physics* **29** (2008) 386–392.
 - [17] Berry Christopher PL and Gair Jonathan R *Linearized $f(R)$ gravity: gravitational radiation and solar system tests*, *Physical Review D—Particles, Fields, Gravitation, and Cosmology* **83** (2011) 104022.
 - [18] Chiba Takeshi, Smith Tristan L and Erickcek Adrienne L *Solar System constraints to general $f(R)$ gravity*, *Physical Review D—Particles, Fields, Gravitation, and Cosmology* **75** (2007) 124014.
 - [19] Guo Jun-Qi *Solar system tests of $f(R)$ gravity*, *International Journal of Modern Physics D* **23** (2014) 1450036.
 - [20] Sokoliuk Oleksii et al., *On the impact of $f(Q)$ gravity on the large scale structure*, *Monthly Notices of the Royal Astronomical Society* **522** (2023) 252–267.
 - [21] Motohashi Hayato and Suyama Teruaki *Third order equations of motion and the Ostrogradsky instability*, *Physical Review D* **91** (2015) 085009.
 - [22] Harko Tiberiu, Lobo Francisco *$f(R, L, m)$ gravity*, *The European Physical Journal C* **70** (2010) 373–379.
 - [23] Wang Jun, Liao Kai *Energy conditions in $f(R, L, m)$ gravity*, *Classical and Quantum Gravity* **29** (2012) 215016.
 - [24] Jaybhaye Lakhani V, Bhattacharjee Snehasish, Sahoo, PK *Baryogenesis in $f(R, L, m)$ gravity*, *Physics of the Dark Universe* **40** (2023) 101223.
 - [25] Maurya Dinesh Chandra *Constrained Λ CDM dark energy models in higher derivative $f(R, L, m)$ -gravity theory*, *Physics of the Dark Universe* **42** (2023) 101373.
 - [26] Singh JK *A constrained cosmological model in $f(R, L, m)$ gravity*, *New Astronomy* **104** (2023) 102070.
 - [27] Myrzakulov Ratbay *FRW cosmology in $f(R, T)$ gravity*, *The European Physical Journal C* **72** (2012) 2203.
 - [28] Bhattacharjee Snehasish, Santos JRL, Moraes PHRS, Sahoo PK *Inflation in $f(R, T)$ gravity*, *The European Physical Journal Plus* **135** (2020) 576.
 - [29] Shabani Hamid, Ziaie Amir Hadi *Stability of the Einstein static universe in $f(R, T)$ gravity*, *The European Physical Journal C* **77** (2017) 1–15.
 - [30] Mishra RK and Sharma Rahul *EXPLORING $f(T)$ GRAVITY DYNAMICS & COSMOLOGICAL PARAMETERS*, *Romanian Journal of Physics* **70** (2025) 1-2.

- [31] Capozziello Salvatore et al., *Cosmography in $f(T)$ gravity* *Physical Review D—Particles, Fields, Gravitation, and Cosmology* **84** (2011) 043527.
- [32] Bahamonde Sebastian, Said Jackson Levi and Zubair M *Solar system tests in modified teleparallel gravity* *Journal of Cosmology and Astroparticle Physics* **2020** (2020) 024.
- [33] Li Baojiu, Sotiriou Thomas P and Barrow John D *Large-scale structure in $f(T)$ gravity*, *Physical Review D—Particles, Fields, Gravitation, and Cosmology* **83** (2011) 104017.
- [34] Sokoliuk Oleksii et al., *On the impact of $f(Q)$ gravity on the large scale structure*, *Monthly Notices of the Royal Astronomical Society* **522** (2023) 252–267.
- [35] Wang Wenyi, Hu Kun and Katsuragawa Taishi *Solar system tests in covariant $f(Q)$ gravity*, *Physical Review D* **111** (2025) 064038.
- [36] Mandal Sanjay et al., *Cosmological observational constraints on the power law $f(Q)$ type modified gravity theory*, *The European Physical Journal C*, **83** (2023) 1141.
- [37] Koussour M and De Avik *Observational constraints on two cosmological models of $f(Q)$ theory*, *The European Physical Journal C*, **83**(2023) 400.
- [38] , Ayuso Ismael, Lazkoz Ruth and Salzano Vincenzo *Observational constraints on cosmological solutions of $f(Q)$ theories*, *Physical review d* **103** (2021) 063505.
- [39] Lazkoz Ruth et al., *Observational constraints of $f(Q)$ gravity*, *Physical Review D* **100**(2019) 104027.
- [40] Motohashi Hayato and Suyama Teruaki *Third order equations of motion and the Ostrogradsky instability*, *Physical Review D*, **91** (2015) 085009.
- [41] Sahl Shambel, de la Cruz-Dombriz Álvaro and Abebe Amare *Structure growth in $f(Q)$ cosmology*, *Monthly Notices of the Royal Astronomical Society*, **539** (2025) 690–703.
- [42] Sami Heba et al., *Covariant density and velocity perturbations of the quasi-Newtonian cosmological model in $f(T)$ gravity*, *The European Physical Journal C*, **81** (2021) 1–17.
- [43] Jiménez Jose Beltrán *Cosmology in $f(Q)$ geometry*, *Physical Review D*, **101** (2020) 103507.
- [44] Xu Yixin *$f(Q, T)$ gravity*, *The European Physical Journal C*, **79**(2019) 1–19.
- [45] Xu Yixin *Weyl type $f(Q, T)$ gravity, and its cosmological implications*, *The European Physical Journal C*, **80** (2020) 1–22.
- [46] Arora Simran *$f(Q, T)$ gravity models with observational constraints*, *Physics of the Dark Universe*, **30** (2020) 100664.
- [47] Arora Simran, Santos JRL and Sahoo PK *Constraining $f(Q, T)$ gravity from energy conditions*, *Physics of the Dark Universe*, **31** (2021) 100790.
- [48] Hazarika Ayush, Arora Simran, Sahoo PK and Harko Tiberiu *$f(Q, \mathcal{L}_m)$ gravity, and its cosmological implications*, *arXiv:2407.00989* (2024)
- [49] Myrzakulov Yerlan et al., *Late-time cosmology in $f(Q, \mathcal{L}_m)$ gravity: Analytical solutions and observational fits* *Physics of the Dark Universe*, **46** 101614.
- [50] Myrzakulov Yerlan et al., *Constraining $f(Q, \mathcal{L}_m)$ gravity with bulk viscosity*, *Physics of the Dark Universe*, (2025) 101829.
- [51] Myrzakulov Kairat *Observational analysis of late-time acceleration in $f(Q, \mathcal{L}_m)$ gravity*, *Journal of High Energy Astrophysics*, **44** (2024) 164–171.
- [52] Jiménez Jose Beltrán, Heisenberg Lavinia and Koivisto Tomi *Coincident general relativity*, *Physical Review D*, **98**(2018) 044048.
- [53] Khyllep Wompherdeiki, Paliathanasis Andronikos and Dutta Jibitesh *Cosmological solutions and growth index of matter perturbations in $f(Q)$ gravity*, *Physical Review D*, **103** (2021) 103521
- [54] Munyeshyaka Albert, Dhankar Praveen Kumar and Ntahompagaze Joseph *Matter power spectrum in a power-law $f(G)$ gravity* *New Astronomy* **102423** (2025) 1384–1076, doi.org/10.1016/j.newast.2025.102423.
- [55] Ntahompagaze Joseph, Abebe Amare and Mbonye Manasse R *Large-scale structure power spectrum from scalar-tensor gravity*, *International Journal of Modern Physics D*, **31** (2022) 2250071.
- [56] Abebe Amare, De la Cruz-Dombriz Alvaro and Dunsby Peter KS *Large scale structure constraints for a class of $f(R)$ theories of gravity*, *Physical Review D—Particles, Fields, Gravitation, and Cosmology*, **88** (2013) 044050.
- [57] Kazantzidis Lavrentios and Perivolaropoulos Leandros *Evolution of the $f\sigma_8$ tension with the Planck 15/Λ CDM determination and implications for modified gravity theories*, *Physical Review D*, **97** (2018) 103503.
- [58] Kazantzidis L et al. *Hints for possible low redshift oscillation around the best-fitting ΛCDM model in the expansion history of the Universe*, *Monthly Notices of the Royal Astronomical Society*, **501** (2021) 3421–3426.
- [59] Kazantzidis Lavrentios and Perivolaropoulos Leandros *σ_8 tension. Is gravity getting weaker at low z ? Observational evidence and theoretical implications*, *Modified Gravity and Cosmology: An Update by the CANTATA Network*, (2021) 507–537.
- [60] Panotopoulos Grigoris and Rincon Angel *Growth of structures and redshift-space distortion data in scale-dependent gravity*, *The European Physical Journal Plus*, **136** (2021) 1–14.
- [61] Nesseris Savvas, Pantazis George and Perivolaropoulos Leandros *Tension and constraints on modified gravity parametrizations of $G_{\text{eff}}(z)$ from growth rate and Planck data*, *Physical Review D*, **96** (2017) 023542.
- [62] Sahl Shambel, De la Cruz-Dombriz Álvaro and Abebe Amare *Structure growth in $f(Q)$ cosmology*, *Monthly Notices of the Royal Astronomical Society*, **539** (2025) 690–703.
- [63] Lifshitz Evgenii Mikhailovich *On the gravitational stability of the expanding universe*, *J. Phys.*, **10** (1946) 116–129.
- [64] Bardeen James M *Gauge-invariant cosmological perturbations*, *Physical Review D*, **22** (1980) 1882.
- [65] Hawking Stephen W *Perturbations of an expanding universe*, *Astrophysical Journal* **145** (1966) 544.
- [66] Ellis George FR and Bruni Marco *Covariant and gauge-invariant approach to cosmological density fluctuations*, *Physical Review D* **40** (1989) 1804.
- [67] Sahl Shambel et al., *Scalar perturbations in $f(T)$ gravity using the $1+3$ covariant approach*, *The European Physical Journal C*, **80** (2020) 422.
- [68] Sami Heba and Abebe Amare *Perturbations of quasi-Newtonian universes in scalar-tensor gravity*, *International Journal of Geometric Methods in Modern Physics*, **18** (2021) 2150158.
- [69] Abebe Amare et al., *Perturbations in bianchi-v spacetimes with varying λ , g and viscous fluids*, *Universe*, **9**

- (2023) 61.
- [70] Munyeshyaka Albert et al., *On 1+ 3 covariant perturbations of the quasi-Newtonian spacetime in modified Gauss–Bonnet gravity*, *International Journal of Modern Physics D*, **32** (2023) 2350053.
 - [71] Munyeshyaka Albert et al., *On covariant perturbations with scalar field in modified Gauss–Bonnet gravity*, *The European Physical Journal C*, **84** (2024) 51.
 - [72] Munyeshyaka Albert et al., *Perturbations in the interacting vacuum*, *International Journal of Geometric Methods in Modern Physics*, **20** (2023) 2350047.
 - [73] Ntahompagaze Joseph et al., *On 1+ 3 covariant perturbation with chaplygin-stiff fluid system in modified Gauss–Bonnet gravity*, *Rwanda Journal of Engineering, Science, Technology and Environment*, **7** (2025) 1.
 - [74] R. Jimenez and A. Loeb, “Constraining cosmological parameters based on relative galaxy ages,” *Astrophys. J.* **573** (2002), 37–42 doi:10.1086/340549 [arXiv:astro-ph/0106145 [astro-ph]].
 - [75] M. Moresco, *Mon. Not. Roy. Astron. Soc.* **450** (2015) no.1, L16–L20 doi:10.1093/mnras/rlv037 [arXiv:1503.01116 [astro-ph.CO]].
 - [76] D. Brout, D. Scolnic, B. Popovic, A. G. Riess, J. Zuntz, R. Kessler, A. Carr, T. M. Davis, S. Hinton and D. Jones, *et al.* *Astrophys. J.* **938** (2022) no.2, 110 doi:10.3847/1538-4357/ac8e04 [arXiv:2202.04077 [astro-ph.CO]].
 - [77] T. M. C. Abbott *et al.* [DES], *Astrophys. J. Lett.* **973** (2024) no.1, L14 doi:10.3847/2041-8213/ad6f9f [arXiv:2401.02929 [astro-ph.CO]].
 - [78] M. Vincenzi *et al.* [DES], *Astrophys. J.* **975** (2024) no.1, 86 doi:10.3847/1538-4357/ad5e6c [arXiv:2401.02945 [astro-ph.CO]].
 - [79] M. Abdul Karim *et al.* [DESI], [arXiv:2503.14738 [astro-ph.CO]].
 - [80] S. Alam *et al.* [eBOSS], *Phys. Rev. D* **103** (2021) no.8, 083533 doi:10.1103/PhysRevD.103.083533 [arXiv:2007.08991 [astro-ph.CO]].
 - [81] A. G. Adame *et al.* [DESI], *JCAP* **02** (2025), 021 doi:10.1088/1475-7516/2025/02/021 [arXiv:2404.03002 [astro-ph.CO]].
 - [82] N. Aghanim *et al.* [Planck], *Astron. Astrophys.* **641** (2020), A6 [erratum: *Astron. Astrophys.* **652** (2021), C4] doi:10.1051/0004-6361/201833910 [arXiv:1807.06209 [astro-ph.CO]].
 - [83] L. Chen, Q. G. Huang and K. Wang, *JCAP* **02** (2019), 028 doi:10.1088/1475-7516/2019/02/028 [arXiv:1808.05724 [astro-ph.CO]].
 - [84] D. Foreman-Mackey, D. W. Hogg, D. Lang and J. Goodman, *Publ. Astron. Soc. Pac.* **125** (2013), 306–312 doi:10.1086/670067 [arXiv:1202.3665 [astro-ph.IM]].
 - [85] A. Lewis, [arXiv:1910.13970 [astro-ph.IM]].
 - [86] Fedeli Cosimo, Dolag K and Moscardini Lauro *Matter power spectra in dynamical dark energy cosmologies*, *Monthly Notices of the Royal Astronomical Society*, **419** (2012) 1588–1602.
 - [87] Munyeshyaka Albert, Dhankar Praveen Kumar and Ntahompagaze Joseph *Matter power spectrum in a power-law $f(G)$ gravity*, *New Astronomy*, **120** (2025) 102423.
 - [88] Mhamdi Dalale et al., *Constraints on power law and exponential models in $f(Q)$ gravity*, *Physics Letters B*, **120** (2025) 102423.
 - [89] Mhamdi Dalale et al., *Cosmological constraints on $f(Q)$ gravity with redshift space distortion data*, *The European Physical Journal C*, **859** (2024) 139113.
 - [90] Albuquerque Inês S and Frusciante Noemi *A designer approach to $f(Q)$ gravity and cosmological implications*, *Physics of the Dark Universe*, **35** (2022) 100980.